ESTIMATES OF THE UNCERTAINTY OF RADIATIVE HEAT FLUX CALCULATED FROM TOTAL HEAT FLUX MEASUREMENTS

by

Rodney Bryant, Erik Johnsson, Thomas Ohlemiller and Carole Womeldorf
Building and Fire Research Laboratory
National Institute of Standards and Technology
Gaithersburg, MD 20899, USA

Reprinted from the Interflam'01. International Fire Science and Engineering Conference, 9th. Proceedings. September 17-19, 2001. Edinburgh, Scotland. 2001.

NIST
National Institute of Standards and Technology
Technology Administration, U.S. Department of Commerce

ESTIMATES OF THE UNCERTAINTY OF RADIATIVE HEAT FLUX CALCULATED FROM TOTAL HEAT FLUX MEASUREMENTS

Rodney Bryant, Erik Johnsson, Thomas Ohlemiller and Carole Womeldorf*
Building and Fire Research Laboratory
National Institute of Standards and Technology
Gaithersburg, MD, USA

ABSTRACT

As part of an effort to characterize the uncertainties associated with heat flux measurements in a fire environment, an uncertainty analysis example was performed using measurement data from a room corner surface products test that followed the guidelines of ISO 9705. Equations to model the heat transfer at the surface of a Schmidt-Boelter (thermopile) type total heat flux gauge were selected for use to calculate the incident radiative flux from a total heat flux measurement. The effects of the heat flux measurement uncertainty sources were evaluated by employing an uncertainty propagation on the resulting equation for incident radiation. For the model equations and the example conditions selected, the free-stream temperature measurement and the heat flux gauge calibration constant were suggested as major uncertainty contributors. The study demonstrates how to systematically identify major sources of uncertainty for the purpose of reducing total uncertainty and therefore enhancing experiment design.

INTRODUCTION

Heat can be transmitted by three modes: convection, conduction, and radiation. Total heat flux gauges are non-ideal and can have responses that are sensitive to each mode. Radiation is a significant mode of heat transfer in typical fire environments; it is particularly important to enclosure fires where its cumulative pre-heating effects accelerate burning and increase the chances of flashover. Though the incident radiation is independent of the measurement, interpretation of the measurement may require knowledge of several parameters. Consequently, the uncertainty associated with a heat flux measurement depends on multiple factors such as the gauge characteristics, the calibration conditions and accuracy, as well as the incident flux modes and magnitudes in the actual measurement situation.[1,2]

Total heat flux gauges are typically employed in fire test measurements. The gauges measure the combined effects of radiation and convection. Therefore, the convective component contributes to the total uncertainty when radiation is the quantity required. Total heat flux gauges can be configured with glass windows to minimize the convective effects, however additional influences and uncertainties are introduced by the optical properties of the glass. Investigations by Robertson and Ohlemiller[3] and Wetterlund and Persson[4] discuss methods to

* Currently, Graduate Research Assistant, Johns Hopkins University, Baltimore, MD.

quantify the convective component for some specific total heat flux measurements. Both investigations report that their methods to partition the heat flux measurements have an approximately 25 % uncertainty.

It is often the case that a physical quantity of interest cannot be measured in a single direct measurement but is instead determined over multiple steps. One or more quantities are measured directly, and the quantity of interest is calculated from them. When a measurement requires multiple steps, the estimation of uncertainty must account for each step. The uncertainties of the direct measurements must be estimated and then it must be determined how each uncertainty propagates through to the final quantity of interest.[5] The physical quantity of interest for this study is incident radiative flux. There exist several types of heat flux gauges capable of responding to the incident radiative flux; for this study only the total heat flux gauge will be considered. Neither total heat flux nor incident radiative flux can be measured directly. Both require indirect measurements, therefore an uncertainty propagation is required to estimate the total measurement uncertainty.

The purpose of the present study is to develop a better understanding of the uncertainties associated with heat flux measurements. Radiant heat flux was selected as the mode of heat transfer for study due to its role in the evaluation of potential fire growth. Equations were selected from the literature to represent the radiative flux incident on a heat flux gauge, and data from a standard fire test were selected to illustrate the partitioning of a total heat flux measurement. Finally, an uncertainty propagation was performed to estimate the total uncertainty of the calculation of incident radiative flux.

MODEL EQUATIONS

For the experimental arrangement to be analyzed here, the heat flux gauge is free standing at the floor and located in the geometric center of the room as described in the details of ISO 9705.[6] The gauge views radiation from the surroundings and is subject to convection from a cross flow in the lower layer of the room as displayed in Figure 1. The cross flow is due to the inflow of air from a doorway located along one wall of the room. A control volume may be defined to encompass the top surface of the gauge. At this surface, the first law of thermodynamics requires the energy entering and leaving the surface to balance. This requirement is exploited to determine indirectly the mode of heat transfer under study, i.e. the incident radiative flux ($q''_{rad,inc}$).

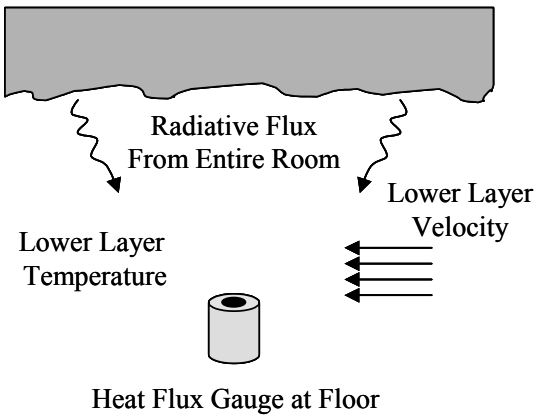

Figure 1 Total heat flux gauge setup for the room corner surface products test.

The gauges required for ISO 9705 are either Gardon (foil) or Schmidt-Boelter (thermopile) type. Both gauge types respond to radiation and convection, though to varying degrees. The response of the Gardon gauge may be nonlinear when subject to mixed mode heat transfer.[7] The description of heat transfer for the Schmidt-Boelter gauge is simpler and it was therefore selected for this study. The Schmidt-Boelter gauge consists of a thin insulating material across which a temperature difference is measured by use of a thermopile or series arrangement of tiny thermocouple junctions. The thermopile is useful for creating a substantial voltage output for a small temperature difference.[8,9]

Energy Balance

Figure 2 displays the sensor surface of the Schmidt-Boelter heat flux gauge, which is subject to radiative heat transfer due to a radiant source and convection due to a cross flow at free-stream velocity and temperature, u_∞ and T_∞, respectively. Heat flow due to both convection and conduction is away from the surface. The surface emits radiation to the surroundings and also reflects a small portion of the incident radiation.

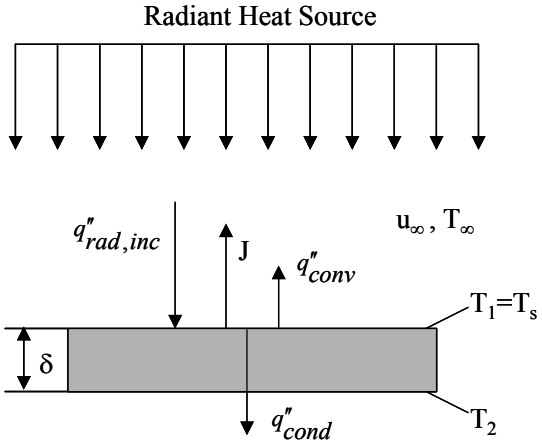

Figure 2 Energy balance at heat flux gauge surface.

Assuming steady-state heat transfer, Arai et al.[10] have described the balance of heat into and away from the surface by Equations 1 and 2.

$$q''_{rad,inc} = J + q''_{conv} + q''_{cond} \qquad (1)$$

where

$$J = (1-\varepsilon_s)q''_{rad,inc} + \varepsilon_s \sigma T_s^4 \qquad (2)$$

is the combination of radiation reflected and emitted from a surface at temperature, T_s. The surface is assumed to be diffuse and gray, therefore the surface emissivity, ε_s, and absorptivity are the same. A typical commercial heat flux gauge actually measures the heat conduction away from the surface. The mode of heat transfer under study, incident radiation, can therefore be calculated using Equation 1 with knowledge of the parameters required to estimate the convective heat transfer.

Convection Estimate

The heat flux gauge surface is circular with diameter, d, however, the convection relation for flow over a flat plate with length, d, is employed as an approximation to estimate convection at the gauge surface. The airflow across the gauge surface is assumed to be laminar. The free-stream flow could be somewhat turbulent but the boundary layer is basically laminar. This is a valid assumption since, for the conditions under study, the Reynolds number at the gauge surface is on the order of 3000, two orders of magnitude less than the critical Reynolds number required for transition to turbulent flow. Because the flow is essentially laminar, it is appropriate to employ an average heat transfer coefficient, h_{avg}, in the convection estimate.[11] The following equation therefore estimates the convective heat flux at the gauge surface.

$$q''_{conv} = h_{avg}\left(T_s - T_\infty\right) = \frac{0.664 u_\infty^{1/2} \,\mathrm{Pr}^{1/3}\, k_g}{\nu^{1/2} d^{1/2}}\left(T_s - T_\infty\right) \qquad (3)$$

Because the gauge is located in the lower layer of the room, it is subject to the air flowing into the enclosure during the fire test. Therefore the fluid properties, thermal conductivity, k_g, kinematic viscosity, ν, and Prandtl number, Pr (ratio of kinematic viscosity and thermal diffusivity) are calculated for air at the film temperature for the gauge surface, $T_f = \frac{1}{2}(T_s + T_\infty)$.

Calibration Relation

Heat flux gauges are typically calibrated with a radiant source, usually a blackbody furnace, traceable to a temperature standard. The result of the calibration is typically a linear relation, Equation 4, between the heat flux gauge output voltage, V_{sensor}, and the incident radiation from the radiant source. The gauge manufacturer supplies the calibration constant, C_{sensor}. Typical commercial gauges measure the conductive heat flux at the surface, q''_{cond}. Therefore the energy balance across the surface in Figure 2 can be applied again, but for the case of a calibration with a radiant source. Convective effects during the calibration are usually assumed to be negligible. Similarly, the radiation emitted from the gauge surface is assumed to be negligible for mid range radiation calibrations.[12] However, the T_s^4 term will be included for the purposes of this study due to the current ability of gauges to record their surface temperature. It may not be practical to match or maintain the gauge surface temperature during actual use at the surface temperature during calibration, therefore the additional subscript of "*cal*" is added. Equation 5 represents the energy balance during calibration with a radiant source and negligible convection effects. Equation 4 can be substituted for incident radiation to form Equation 6, the relation between the actual gauge measurement, conduction, and the calibration results.

$$q''_{rad,inc,cal} = C_{sensor} V_{sensor} \qquad (4)$$

$$q''_{cond} = \varepsilon_s q''_{rad,inc,cal} - \varepsilon_s \sigma T_{s,cal}^4 \qquad (5)$$

$$q''_{cond} = \varepsilon_s C_{sensor} V_{sensor} - \varepsilon_s \sigma T_{s,cal}^4 \qquad (6)$$

Incident Radiation

Combining Equations 1, 2, 3 and 6 completes the expression for the calculation of incident radiation from a total heat flux gauge measurement and is given by:

$$q''_{rad,inc} = \frac{1}{\varepsilon_s}\left[\varepsilon_s \sigma T_s^4 + \frac{0.664 u_\infty^{1/2} \Pr^{1/3} k_g}{\nu^{1/2} d^{1/2}}\left(T_s - T_\infty\right) + \varepsilon_s C_{sensor} V_{sensor} - \varepsilon_s \sigma T_{s,cal}^4\right] \quad (7)$$

The accuracy of temperature, velocity, voltage, and calibration measurements and the estimates of relevant fluid properties will determine the accuracy of the incident radiation measurement. Equation 7 represents an attempt to calculate the incident radiation from total heat flux gauge measurements. The uncertainty of the inferred incident radiation can be estimated by applying an uncertainty propagation to this relation.

UNCERTAINTY ANALYSIS

Suppose a set of measurements is made to determine the result, R. The result can be expressed as a function of the independent variables, some of which are the direct measurements.

$$R = R(x_1, x_2, x_3, ...x_n) \quad (8)$$

The uncertainty of the result will be denoted as w_R, and the uncertainty of the independent variables as $w_1, w_2, w_3, ..., w_n$. If the uncertainties of the independent variables are uncorrelated, their contribution to the total uncertainty of the result can be determined by applying the uncertainty propagation given by Equation 9.[5,9,13]

$$w_R = \left[\left(\frac{\partial R}{\partial x_1} w_1\right)^2 + \left(\frac{\partial R}{\partial x_2} w_2\right)^2 + ... + \left(\frac{\partial R}{\partial x_n} w_n\right)^2\right]^{1/2} \quad (9)$$

The partial derivatives are often described as sensitivity coefficients. They determine the contribution of uncertainty for their associated variable to the overall uncertainty. Uncertainty propagation is very useful in experimental design to isolate variables that are significant contributors to the overall uncertainty of the desired result.

The result under study, incident radiative flux, has been expressed as a function of several variables, all of which are assumed to be independent with uncorrelated individual uncertainties. Several of the variables, such as gauge output voltage, surface temperature, surface diameter, free-stream temperature and velocity, can be measured directly. Other variables are given as constants or are estimated from reference tables.

Applying Equation 9 to Equation 7, the general expression for the absolute uncertainty of the incident radiative flux measurement is:

$$w_{q''_{rad,inc}} = \left[\begin{array}{l} (\frac{\partial q''_{rad,inc}}{\partial \varepsilon_s} w_{\varepsilon_s})^2 + (\frac{\partial q''_{rad,inc}}{\partial C_{sensor}} w_{C_{sensorr}})^2 + (\frac{\partial q''_{rad,inc}}{\partial V_{sensor}} w_{V_{sensor}})^2 + \\ (\frac{\partial q''_{rad,inc}}{\partial T_{s,cal}} w_{T_{s,cal}})^2 + (\frac{\partial q''_{rad,inc}}{\partial T_s} w_{T_s})^2 + (\frac{\partial q''_{rad,inc}}{\partial u_\infty} w_{u_\infty})^2 + \\ (\frac{\partial q''_{rad,inc}}{\partial \Pr} w_{\Pr})^2 + (\frac{\partial q''_{rad,inc}}{\partial d} w_d)^2 + (\frac{\partial q''_{rad,inc}}{\partial T_\infty} w_{T_\infty})^2 \end{array} \right]^{1/2} \quad (10)$$

Both the gas conductivity and kinematic viscosity are functions of gas temperature, and the tabulated data can be expressed as polynomial fits. Therefore both gas properties are entered into Equation 7 as expressions of the film temperature and their partial derivative is computed with respect to the surface and free-stream temperature. The Prandtl number has negligible variation for the entire range of experimental conditions and it is therefore assumed to be constant. Equation 10 becomes the general expression for the relative uncertainty when it is divided by $q''_{rad,inc}$. Equations 11 - 19 represent the partial derivative terms or the sensitivity coefficients. Note that the full differentiation of the gas property relations for gas conductivity and kinematic viscosity are not included in Equations 15 and 19 for brevity.

$$\frac{\partial q''_{rad,inc}}{\partial \varepsilon_s} = \frac{-0.664 \Pr^{1/3} \sqrt{u_\infty} k_g (T_s - T_\infty)}{\varepsilon_s^2 \sqrt{d\nu}} \quad (11)$$

$$\frac{\partial q''_{rad,inc}}{\partial C_{sensor}} = V_{sensor} \quad (12)$$

$$\frac{\partial q''_{rad,inc}}{\partial V_{sensor}} = C_{sensor} \quad (13)$$

$$\frac{\partial q''_{rad,inc}}{\partial T_{s,cal}} = -4\sigma T_{s,cal}^3 \quad (14)$$

$$\frac{\partial q''_{rad,inc}}{\partial T_s} = \frac{0.664 \Pr^{1/3} \sqrt{u_\infty}}{\varepsilon_s \sqrt{d\nu}} \left[k_g + \frac{\partial k_g}{\partial T_s}(T_s - T_\infty) - \frac{k_g}{2\nu} \frac{\partial \nu}{\partial T_s}(T_s - T_\infty) \right] + 4\sigma T_s^3 \quad (15)$$

$$\frac{\partial q''_{rad,inc}}{\partial u_\infty} = \frac{0.332 \Pr^{1/3} k_g (T_s - T_\infty)}{\varepsilon_s \sqrt{d u_\infty \nu}} \quad (16)$$

$$\frac{\partial q''_{rad,inc}}{\partial \Pr} = \frac{0.221 k_g (T_s - T_\infty) \sqrt{u_\infty}}{\Pr^{2/3} \varepsilon_s \sqrt{d\nu}} \quad (17)$$

$$\frac{\partial q''_{rad,inc}}{\partial d} = \frac{-0.332 \Pr^{1/3} k_g (T_s - T_\infty) \sqrt{u_\infty}}{d^{3/2} \varepsilon_s \sqrt{\nu}} \quad (18)$$

$$\frac{\partial q''_{rad,inc}}{\partial T_\infty} = \frac{0.664\,\mathrm{Pr}^{1/3}\sqrt{u_\infty}}{\varepsilon_s\sqrt{d\nu}}\left[\frac{\partial k_g}{\partial T_\infty}(T_s - T_\infty) - k_g - \frac{k_g}{2\nu}\frac{\partial \nu}{\partial T_\infty}(T_s - T_\infty)\right] \quad (19)$$

APPLICATION EXAMPLE

The ISO 9705 - Full-Scale Room Test for Surface Products is designed to evaluate the contribution to fire growth by wall or ceiling surface products.[6] Several principle measurements, such as total heat flux, total heat release rate, gas composition, and optical density, may be conducted to evaluate the potential hazards of the fire. The measurement of interest for this study is total heat flux. By measuring total heat flux incident on a heat flux gauge at the center of the floor, the test provides a measure of the potential for fire spread to other objects within the room, but remote from the ignition source. The standard recognizes that the total heat flux measurement consists of heat transfer contributions from both radiation and convection with the major component being radiation. The standard also suggests measurements of gas temperature in the room and velocity through the doorway if additional information is required. For the present study, such measurements are necessary for estimating the convective heat transfer. For the reasons mentioned, heat flux measurements from the ISO 9705 or similar tests serve as excellent examples of fire-environment total heat flux measurements with existing potential for partitioning of the modes of heat transfer.

A series of large-scale room fire experiments was conducted at the Technical Research Centre of Finland.[14] The test room had 6 times more surface area than a similar room required by ISO 9705. The purpose of the tests was to compare the performance of surface products with their performance in smaller scale tests, specifically ISO 9705. Because the tests followed the procedure of ISO 9705 as much as possible they were selected as an appropriate source of data for this study. The data were used to illustrate the calculation of incident radiative flux from the total heat flux measurement, Equation 7, and to estimate the uncertainty of the calculation using Equation 10. Measurement data of total heat flux at the floor, lower layer gas temperature at the doorway and lower layer velocity at the doorway serve as input for the calculation. The surface product test selected, a combustible facing on mineral wool, demonstrated total floor heat fluxes ranging from low levels to heat flux levels typical of flashover conditions.

Estimates of the input parameters for Equation 7 and their uncertainties are listed in Table 1. Variables are taken directly from the product test data or inferred directly from the data as in the case of the gauge output voltage. Estimated values for the gauge surface emissivity and the gauge calibration constant were assumed from manufacturer specifications. Estimated values for the gauge surface temperature and the gauge diameter were assumed from the requirements of ISO 9705. Though not stated in ISO 9705, it was assumed that each uncertainty estimate was modeled by a normal probability distribution and represents a 67 % probability that the parameter value lies in the interval $w_{i,-}$ to $w_{i,+}$. Similar assumptions were made for the remaining uncertainty estimates. Because the parameter uncertainty estimates are based on manufacturer's specifications, data from reports, or general knowledge, Taylor and Kuyatt[15] classify them as Type B uncertainties. The estimates of uncertainty listed in Table 1 are established as a baseline.

It is important to note that the data of lower layer temperature and velocity measurements at the doorway serve as estimates for the free-stream temperature and free-stream velocity near the heat flux gauge. Such estimates are required for the calculation of convective heat flux, Equation 3. Since actual measurements of free-stream temperature and velocity near the gauge are not available, the reader is reminded that the analysis is an approximation of radiative heat flux and an illustration of the process of uncertainty propagation.

Table 1 Input Parameter and Uncertainty Estimates

Parameter	Estimate	Relative Uncertainty
ε_s	0.96[*]	3.0 %[*]
C_{sensor}	5132 [W/m^2 mV][*]	3.0 %[*]
V_{sensor}	Variable [mV][†]	0.5 %[†]
$T_{s,cal}$	295 [K][§]	1.0 %[§]
T_s	297 [K][†]	2.0 %[†]
u_∞	Variable [m/s][†]	20 %[†]
Pr	0.7[§]	1.0 %[§]
D	0.025 [m][†]	1.0 %[§]
T_∞	Variable [K][†]	10 %[‡]
Source: [*]Manufacturer specifications, [†]ISO 9705, [‡]Published report (see reference 16), [§]General knowledge		

Figure 3 demonstrates the time history of both the measured total heat flux and the calculated incident radiative flux from Equation 7 on the primary y-axis. The absolute uncertainty is displayed as error bars on the flux curve while the relative uncertainty is displayed on the secondary y-axis. Results at times greater than 600 s are displayed because the heat flux levels prior to this period are small and sometimes negative due to cooling of the heat flux gauge by the cross flow. The difference between the total heat flux measured and the calculated incident radiative flux is less than 5 %. This agrees with ISO 9705, which assumes radiation to be the main component of the total heat flux measurement. The estimated relative uncertainty of the calculation of incident radiative flux is 20 % or greater for total heat flux measurements below 2400 W/m^2. For higher total heat flux measurements the estimated relative uncertainty ranges from 6 % to 20 %, demonstrating a decrease with respect to increasing total heat flux.

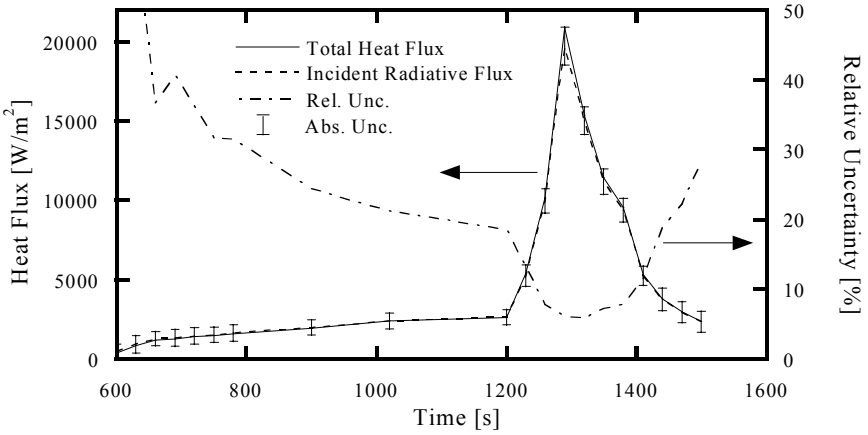

Figure 3 Total heat flux measurements taken from a room corner surface products test and the calculated incident radiative flux and its estimated uncertainty.

Figure 4 displays again the estimated relative uncertainty of the calculated incident radiative flux. In addition, the relative uncertainty attributed to the individual parameters is displayed, as inferred from Equation 10. Because the total relative uncertainty varies as the root mean square of the individual uncertainties, parameters with the largest uncertainties tend to contribute more heavily to the total. The uncertainty of the free-stream temperature measurement, the gauge surface temperature measurement and the calibration constant are the most significant contributors to the total estimated uncertainty. The remaining parameters' uncertainties are relatively constant and insignificant over the test conditions. For heat flux levels below 5000 W/m^2, the order of the uncertainty contribution from the top three sources is: 1) the free-stream temperature measurement, 2) the gauge surface temperature measurement, and 3) the calibration constant. At higher total heat flux levels, the uncertainty contribution from the calibration constant replaces the gauge surface temperature measurement as the second highest contributor and demonstrates a potential to compete with the free-stream temperature measurement as the highest contributor of uncertainty. To reduce the overall estimated uncertainty for situations similar to this test case, efforts should focus on reducing the uncertainty of the free-stream temperature measurement and of the calibration constant.

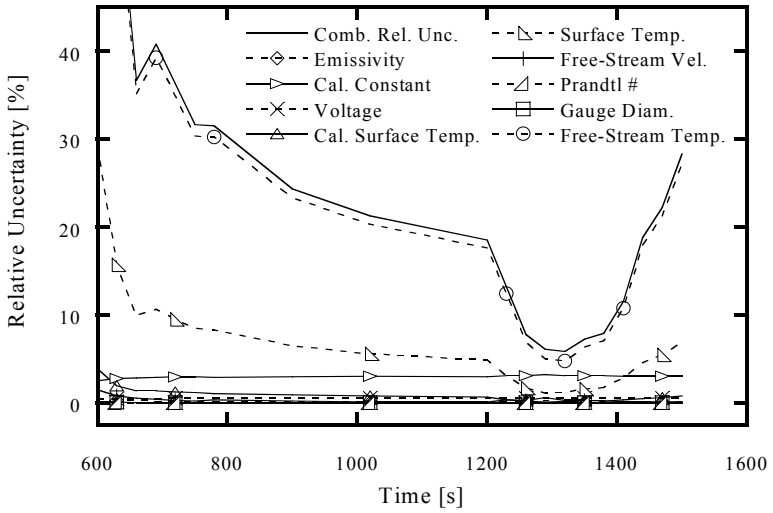

Figure 4 Total relative uncertainty and the parameter uncertainty contribution.

The magnitudes of the sensitivity coefficients are displayed in Table 2. The range of the squared values of the sensitivity coefficients extends over nine orders of magnitude (10^{-1} to 10^{7}). Gauge output voltage, gauge diameter, free-stream velocity and gauge surface emissivity have the largest squared values of partial derivative terms for the low heat flux levels (time less than 1200 s). At high heat flux levels, the same sensitivity coefficients dominate but the order of ranking changes. The results of Figure 4 and Table 2 demonstrate that the order of contribution of parameter uncertainty does not entirely correlate with the order of magnitude of the sensitivity coefficients. The free-stream temperature measurement serves as an example; it contributes significantly to the total uncertainty but is weighted by one of the smaller sensitivity coefficients. The absolute uncertainty of the free-stream temperature measurement is large and is therefore the reason for its significant contribution to the total uncertainty. In this illustration, the parameters with the largest sensitivity

coefficients possess the smallest absolute uncertainty, therefore negating the potential for a large contribution to the total uncertainty.

Table 2 Magnitude of Sensitivity Coefficients

x_i	$\left(\partial q''_{rad,inc} / \partial x_i\right)^2$	
	Low Heat Flux 600 s to 1200 s	**High Heat Flux 1200 s to 1500 s**
ε_s	$2.4\text{x}10^{3}$	$1.7\text{x}10^{5}$
C_{sensor}	$1.0\text{x}10^{-1}$	$3.8\text{x}10^{0}$
V_{sensor}	$2.6\text{x}10^{7}$	$2.6\text{x}10^{7}$
$T_{s,cal}$	$3.4\text{x}10^{1}$	$3.4\text{x}10^{1}$
T_s	$5.0\text{x}10^{2}$	$7.8\text{x}10^{2}$
u_∞	$3.2\text{x}10^{3}$	$3.0\text{x}10^{4}$
Pr	$4.9\text{x}10^{2}$	$3.5\text{x}10^{4}$
d	$8.7\text{x}10^{5}$	$6.1\text{x}10^{7}$
T_∞	$2.7\text{x}10^{2}$	$4.8\text{x}10^{2}$

A further example of the effects of reducing the parameter uncertainty is demonstrated in Figure 5. The baseline case estimates the relative uncertainty of the free-stream temperature measurement at 10 %. This estimate comes from a study to determine the error of aspirated thermocouple measurements in enclosure fires.[16] Reducing this uncertainty by a factor of two greatly reduces the total uncertainty as displayed in Figure 5, Example 2. The effects are the greatest for the lower total heat flux measurements (time less than 1200 s). At higher total heat flux measurements (1200 s to 1400 s), the uncertainty of the calibration constant becomes the major uncertainty contributor in Example 2. Figure 5, Example 3, displays how further reduction of the total uncertainty should focus on reducing the uncertainty of the calibration constant.

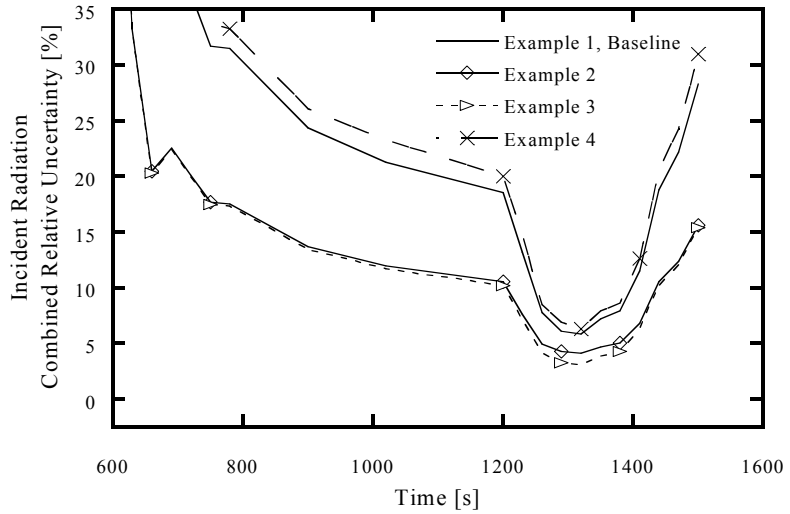

Figure 5 Effects of reducing parameter uncertainty and parameter constants. Example 1: $w_{T\infty}$=.1T_∞, $w_{Csensor}$=.03C_{sensor}, d=0.025 m, Example 2: $w_{T\infty}$=.05T_∞, $w_{Csensor}$=.03C_{sensor}, d=0.025 m, Example 3: $w_{T\infty}$=.05T_∞, $w_{Csensor}$=.015C_{sensor}, d=0.025 m, Example 4: $w_{T\infty}$=.05T_∞, $w_{Csensor}$=.03C_{sensor}, d=0.006 m.

Changing the values of the constant input parameters, such as surface emissivity, calibration constant and surface temperature, resulted in a negligible effect on the total relative uncertainty. However changing the diameter of the heat flux gauge surface did result in notable effects. Comparing Figure 5, Examples 2 and 4: decreasing the gauge surface diameter by a factor of 4 greatly increased the total relative uncertainty. This was due to an increase in the free-stream temperature sensitivity coefficient caused by the reduced diameter as demonstrated in Equation 19. The reduced diameter also causes the convection component to increase as demonstrated in Equation 3. These results suggest that larger Schmidt-Boelter gauges will have less heat transfer contribution from convection and less total uncertainty, since the average boundary layer will be thicker.

Recall that the convection heat transfer coefficient in Equation 3 was taken from the result for flow over a flat plate. A simple comparison of the total relative uncertainty was performed with heat transfer coefficients for other geometries similar to the heat flux gauge. One such appropriate geometry is a finite cylinder in a cross flow. The average heat transfer coefficient is approximately equal to that for the flat plate geometry, however it is the heat transfer coefficient for the end of the cylinder that is of interest. It was determined that the heat transfer coefficients for other geometries such as a square cylinder and a vertical flat plate give a range of coefficients to sufficiently set bounding extremes.[11] The heat transfer coefficient for the square cylinder is a factor of two less than for the horizontal flat plate while the heat transfer coefficient for the vertical flat plate is a factor of two greater. In both cases the total relative uncertainty is reduced or increased, respectively, by a factor of two also. The one-to-one relationship between the heat transfer coefficient and the total relative uncertainty may be attributed to the occurrence of the heat transfer coefficient in the sensitivity coefficient for the free-stream temperature (see Equation 19), a major source of uncertainty.

CONCLUSIONS

The present study illustrates a method to calculate incident radiative flux from a total heat flux measurement and subsequently how to estimate the total uncertainty of the calculation by applying an uncertainty propagation. Data from a room corner surface products test, similar to the ISO 9705, were employed as an example to illustrate the incident radiative flux calculation and the uncertainty analysis. The analysis only approximated the incident radiative flux because required input parameters such as free-stream temperature and free-stream velocity near the heat flux gauge were estimated from measurements in the doorway. The convective heat transfer correlation is also an approximation based on empirical results. However, the results demonstrated that radiative heat transfer is the dominant mode of heat transfer for the total heat flux measurement as implemented in ISO 9705. The results also suggest that the total heat flux measurement can be partitioned to infer the incident radiation with an estimated relative uncertainty of less than 20 %. Estimates with uncertainties as low as 6 % are suggested for heat flux levels near flashover conditions. The uncertainty analysis demonstrates how major sources of uncertainty can be identified and evaluated to reduce the total uncertainty. Based on the model equations selected and the conditions of the example room corner surface products test, the free-stream temperature measurement and the heat flux gauge calibration constant were identified as the major sources of uncertainty. The heat flux gauge surface diameter was also identified as a parameter that can adversely affect the uncertainty estimate.

More complex measurements, such as heat flux gauges embedded in burning objects, also require uncertainty estimates and, if possible, partitioning of heat transfer modes. The present study begins to enhance the understanding of the challenges of performing such heat flux measurements accurately. Future work should focus on applying the approach described here to calculate uncertainties implicit in these more complex heat flux measurement situations. This can provide guidance on the best approach to such measurements.

---

1 Holmberg, D. G., Womeldorf, C. A., Grosshandler, W. L., "Design and Uncertainty Analysis of a Second-Generation Convective Heat Flux Calibration Facility," *Proceedings of the ASME Heat Transfer Division*, **4**, 65-70, (1999).

2 Holmberg, D. G., Womeldorf, C. A., "Performance and Modeling of Heat Flux Sensors in Different Environments," *Proceedings of the ASME Heat Transfer Division*, **4**, 71-77, (1999).

3 Robertson, A. F., Ohlemiller, T. J., "Low Heat-flux Measurements: Some Precautions," *Fire Safety Journal*, **25**, 109-124, (1995).

4 Wetterlund, I., Persson, B., "Calibration and Use of Heat Flux Meters," *Proceedings of the 8th International Interflam Conference*, Edinburgh, Scotland, 35-46, (1999).

5 Taylor, J. R., *An Introduction to Error Analysis – The Study of Uncertainties in Physical Measurements*, University Science Books, Sausalito, California, (1997).

6 ISO 9705, "Fire Tests – Full-Scale Room Test for Surface Products," Geneva, (1993).

7 Borell, G. J., Diller, T. E., "A Convection Calibration Method for Local Heat Flux Gages," *Journal of Heat Transfer*, **109**, 83-89, (1987).

8 Kidd, C. T., Nelson, C. G., "How the Schmidt-Boelter Gage Really Works," *Proceedings of the 41st International Instrumentation Symposium*, Instrument Society of America, Aurora, Colorado, (1995).

9 Holman, J. P., Gajda, W. J., *Experimental Methods for Engineers*, McGraw-Hill, New York, (1984).

10 Arai, N., Matsunami, A., Churchill, S. W., "A Review of Measurements of Heat Flux Density Applicable to the Field of Combustion," *Exp. Thermal and Fluid Science*, **12**, 452-460, (1996).

11 Incropera, F. P., De Witt, D. P., *Introduction to Heat Transfer*, John Wiley & Sons, New York, (1990).

12 "General Description of Radiant Calibration Procedures for Heat Flux Transducers and Infrared Radiometers," MEDTHERM Procedure No. PI-20, (1996).

13 Kline, S. J., "The Purposes of Uncertainty Analysis," *Journal of Fluids Engineering*, **107**, 153-160, (1985).

14 Kokkala, M., Goransson, U., Soderbom, J., "Five Large-Scale Room Fire Experiments – Project 3 of the EUREFIC Fire Research Programme," Technical Research Centre of Finland, VTT 104, (1992).

15 Taylor, B. N., Kuyatt, C. E., "Guidelines for Evaluating and Expressing the Uncertainty of NIST Measurement Results," National Institute of Standards and Technology Technical Note 1297, (1994).

16 Blevins, L. G., Pitts, W. M., "Modeling of Bare and Aspirated Thermocouples in Compartment Fires," *Fire Safety Journal*, **33**, 239-259, (1999).